Research paper

Bioderived dyes-mediated vat photopolymerization 3D printing of chitosan hydrogels for tissue engineering

Michael Zanon [a], Raquel Cue-López [b,c], Enrique Martínez-Campos [b,c], Paula Bosch [c], Davy-Louis Versace [d], Hassan Hayek [d], Nadia Garino [a], Candido Fabrizio Pirri [a], Marco Sangermano [a], Annalisa Chiappone [e,*]

[a] Dipartimento di Scienza Applicata e Tecnologia, Politecnico di Torino, C.so Duca degli Abruzzi 24, 10129 Turin, Italy
[b] Grupo de Síntesis Orgánica y Bioevaluación, Instituto Pluridisciplinar (UCM), Unidad Asociada al ICTP, IQM (CSIC), Paseo de Juan XXIII 1, Madrid 28040, Spain
[c] Departamento de Química Macromolecular Aplicada, Instituto de Ciencia y Tecnología de Polímeros, Consejo Superior de Investigaciones Científicas (CSIC), C/Juan de la Cierva 3, Madrid 28006, Spain
[d] Institut de Chimie et des Matériaux Paris-Est (ICMPE), UMR CNRS-UPEC 7182, 2-8 rue Henri Dunant, Thiais 94320, France
[e] Dipartimento di Scienze Chimiche e Geologiche, Università degli studi di Cagliari, Cittadella Universitaria Blocco D, S.S. 554 bivio per Sestu 09042 Monserrato, CA, Italy

ARTICLE INFO

ABSTRACT

The importance of 3D printable hydrogels is constantly increasing in the field of tissue engineering, due to their characteristic structure and similarity with the human body extracellular matrix (ECM). Herein, Quinizarin-based bioderived photoactive dyes were employed for the 3D printing of methacrylated chitosan by vat photopolymerization (VPP).

Dyes are commonly needed in VPP to obtain good resolution avoiding the light scattering in the vat, here the bioderived molecules had further utility granting the printability with good resolution while acting both as photosensitizers and fillers/crosslinkers. Defined and detailed architectures in the range of millimetres were obtained with low printing times showing for the first time the possibility to obtain all-chitosan 3D structures with suspended features by Digital Light Processing (DLP), which is a form of vat photopolymerization; such a result is not achievable without the quinizarin-derived dyes. The same structures were achieved with an optimized concentration of poly(ethylene glycol) diacrylate, as a comparison, enhancing the resolution. For all the formulations, the important feature to obtain the gel printability (considering reactiveness, viscosity, shear thinning behaviour, mechanical properties and stability) were evaluated. The hydrogels mechanical characterization and swelling properties were also tested and reported. Lastly, the possible application in tissue engineering was also evaluated through cell proliferation analysis over samples, including metabolic activity and DNA contempt assays.

The use of such bioderived photoactive molecules that simultaneously act as photosensitizer enhancing the ink reactivity, as dye improving the definition of the final structures and as filler/crosslinker increasing the mechanical stability, could represent a valuable route for the DLP printing of soft hydrogels.

1. Introduction

3D printing is an advanced and promising technology able to fabricate customized structures through a computer-aided design (CAD) [1–3]. Since Chuck Hull introduced in the 1980s the first 3D printing apparatus, that was the first form of vat photopolymerization technology (stereolithography) [4], many researchers put their efforts to improve and develop new features to widen its applicability in many fields, from electronics, to aerospace [5–8], to medical devices or tissue engineering [9,10]. Especially in tissue engineering applications, 3D printing can become vitally important due to its ability to recreate and mimic perfectly a large variety of damaged patient tissues, even with interconnected and complex porous structures (i.e. heart models [11], vascular networks [12] or pulmonary systems[13]). Moreover, the total worldwide market for additive manufacturing materials forecast to grow up to $23 billion by 2029 [3]. Among these materials most of the sales

belong to polymers, and within them, natural polymers hydrogels are one of the best candidates for scaffolds, due to their extreme similarity to the human body extracellular matrix (ECM) [14–16]. Chitosan, a polysaccharide derived from the deacetylation of chitin, is one of the most used natural polymers thanks to its biocompatibility, biodegradability, availability, anti-inflammatory activity, antioxidant effect, and the possibility to diminish the foreign body reaction with little or totally absent fibrous encapsulation [17]. Nowadays, functionalized chitosan hydrogels are widely used and investigated for many different tissues and applications [18–20], often modified with photo reactive groups (especially with methacrylic groups). In fact, photopolymerization presents many advantages, including fast and effective polymerization, good spatiotemporal control of the hydrogel formation, and the possibility to perform the reaction at room temperature and under physiological conditions [3]. These same characteristics made also light-based 3D printing extremely suitable for the production of hydrogels with complex geometries. Chitosan was already investigated as bio-ink in 3D printing but generally employing material-extrusion printers [21–26], with limitation regarding the ink viscosity or reactiveness [27] and leading to simple structures (such as grids or simple 2D figures). In contrast, vat photopolymerization printers enable the fabrication layer-by-layer of the entire construct with less marked interfaces (unlike the line-by-line method of extrusion-based printers), low printing times and high resolutions [28,29]. Digital light processing (DLP) printers belong to this last category, and unlike stereolithography (SLA) printers, permit the creation of the entire layer "all-at-once" decreasing the printing times but maintaining a great resolution of the final object [30]. Methacrylated chitosan can form a chemically crosslinked hydrogel by photopolymerization but the low degree of substitutions achievable (DS % in a range of 20–33 [18,31–33]) and the limited solubility in water [32] make it hardly processable by DLP printing, above all for the production of complex structures. To the best of our knowledge, one example of all-chitosan DLP printed objects is present in literature building simple structures with no suspended [33]. As an alternative, many studies in the last years focused on the addition of crosslinkers to allow the 3D printing with this technology, such as acrylamide [34] or poly-(ethylene glycol) diacrylate [35].

Beside the monomers' structures, in vat photopolymerization 3D printing, photoinitiators and dyes are extremely important to determine the reactivity and to prevent light scattering, increasing the resolution of the printed structure [5,36]. Lately, two new bio-based methacrylated photoactive dyes were synthetized by Breloy et al. [37] starting from quinizarin, a molecule which is extracted in low concentration from the madder plant roots. The two quinone-like molecules, one mono-methacrylated (Q-1MAc) and one di-methacrylated (Q-2MAc), showed good antimicrobial activity under light activation and the possibility to create radicals upon visible light irradiation when combined with oxidative or reductive agents, concretely acting as photo-initiating systems. The methacrylation performed on quinizarin has the additional advantage of permitting the crosslinking between methacrylated macromolecular chains while avoiding their leaching from the materials once the scaffold is created and their possible cytotoxic interaction with the cell's membranes [38,39]. Herein, the successful DLP printability of all-metacrylated chitosan formulations containing the quinizarin derivatives is shown and compared to a hybrid formulation based on polyethylene glycol diacrylate/methacrylated chitosan also loaded with the quinizarin derivatives. EPR experiments have been performed to clearly understand the methacrylated-dyes photoinitiating properties.

It was demonstrated that a low concentration of dyes, combined with their photo-activity, can replace the addition of synthetic crosslinkers accelerating the polymerization kinetics of methacrylated chitosan and improving, at the same time, the mechanical properties of the final hydrogels. This enables the fast and precise DLP printing of chitosan-based hydrogels, otherwise not achievable without the presence of synthetic quinizarin crosslinkers, with a good resolution of the obtained objects Furthermore, the obtained 3D materials are not cytotoxic and

allow the cells adhesion and proliferation, resulting in promising candidates for tissue engineering applications. The use of such bioderived, photoactive molecules can enlarge the possibilities to obtain DLP printed biobased hydrogels.

2. Materials and Methods

Materials

Chitosan medium molecular weight (CH, Mw = 190–310 kDa, 75–85 % degree of *N*-deacetylation), methacrylic anhydride (MA, 94 %), acetic acid (99 %), dialysis sacks (Avg. flat width 35 mm, MWCO 12 000 Da), Poly(ethylene glycol) diacrylate (PEGDA, average Mn 700), Brilliant Green (BG, hydrogen sulfonate Mw 482.63), lithium phenyl-2,4,6 trimethylbenzoylphosphinate (LAP, $\geq$ 95 %), Dimethyl sulfoxide (DMSO, anhydrous $\geq$ 99.9 %), Quinizarin (QZ, 96 %), *N*-dimethylaminopyridine (DMAP, > 99 %) and 5,5-dimethyl-1-pyrroline *N*-oxide (DMPO) were all purchased from Sigma-Aldrich and used as received without further purification.

Synthesis of methacrylated chitosan

Chiatosan (1,5 % wt) was dissolved in a 2 wt. % acetic acid-deionized (DI) water solution and subsequently it was successfully methacrylated (CHI-MA) following a previous reported work [32]. Briefly, methacrylic anhydride was added at a molar ratio 1:1 with the amino-glucose ring of chitosan and the solution was transferred into a 100 mL clamped Teflon reactor, equipped with pressure and temperature probes, and placed into a microwave furnace (Milestone START Synth, Milestone Inc., Shelton, Connecticut). Reaction parameters: maximum power of 800 W, temperature 80 °C, launch time 60 s and reaction time 10 min. The solution was then cooled back down to ambient temperature, dialyzed for 7 days against DI water and freeze-dried. The ^{1}H NMR spectra proved a degree of methacrylation of 24 % (Fig. S1, SI).

Synthesis of mono/di-methacrylated quinizarin (Q-1MAc and Q-2MAc)

Both quinizarin derivatives dyes have been synthesized according to the previously reported investigation [37]. Q-1MAc was prepared with a final yield of 44 % while Q-2MAc had a yeld of 59 %. The ^{1}H NMR spectra of the synthesized dyes are displayed in Supporting information (Figs. S2-S3, SI).

Hydrogels preparation via photo-crosslinking

Q-1MAc and Q-2MAc were dissolved in a solution of DI water and DMSO (3:1 H_2O:DMSO, $3*10^{-4}$ M) priorly to the addition of freeze-dried CHI-MA (DS % 24, 2 wt. %) and eventually PEGDA (2 wt. %). Then, LAP ($3*10^{-4}$ M) and PEGDA (at different concentrations) were eventually added, and the mixture was stirred until a homogeneous solution was reached. The formulation was poured into PDMS moulds ($\approx$ height = 3 mm, diameter = 5 mm) and irradiated for 5 min with a visible light Hamamatsu LC8 lamp with a cut-off filter below 400 nm equipped with a light guide (50 mW/cm^2).

NMR characterization. NMR spectra were measured on a Bruker Avance II instrument with a frequency of 400 MHz for ^{1}H NMR.

UV-Vis spectroscopy measurements. Absorption spectra of the methacrylated molecules at a concentration of 10^{-4} M in a Water:DMSO solution (3:1, v/v) were collected using a Synergy HTX Multi-Mode Microplate Reader instrument (BioTek, Winooski, VM, USA) set in spectrum mode in the range between 300 and 700 nm and at a scan step of 10 nm.

Electron Paramagnetic resonance (EPR) spin-trapping experiments. EPR spin-trapping experiments have been performed with the EMX spectrometer (standard TE$_{102}$ rectangular cavity (ER 4102 ST,
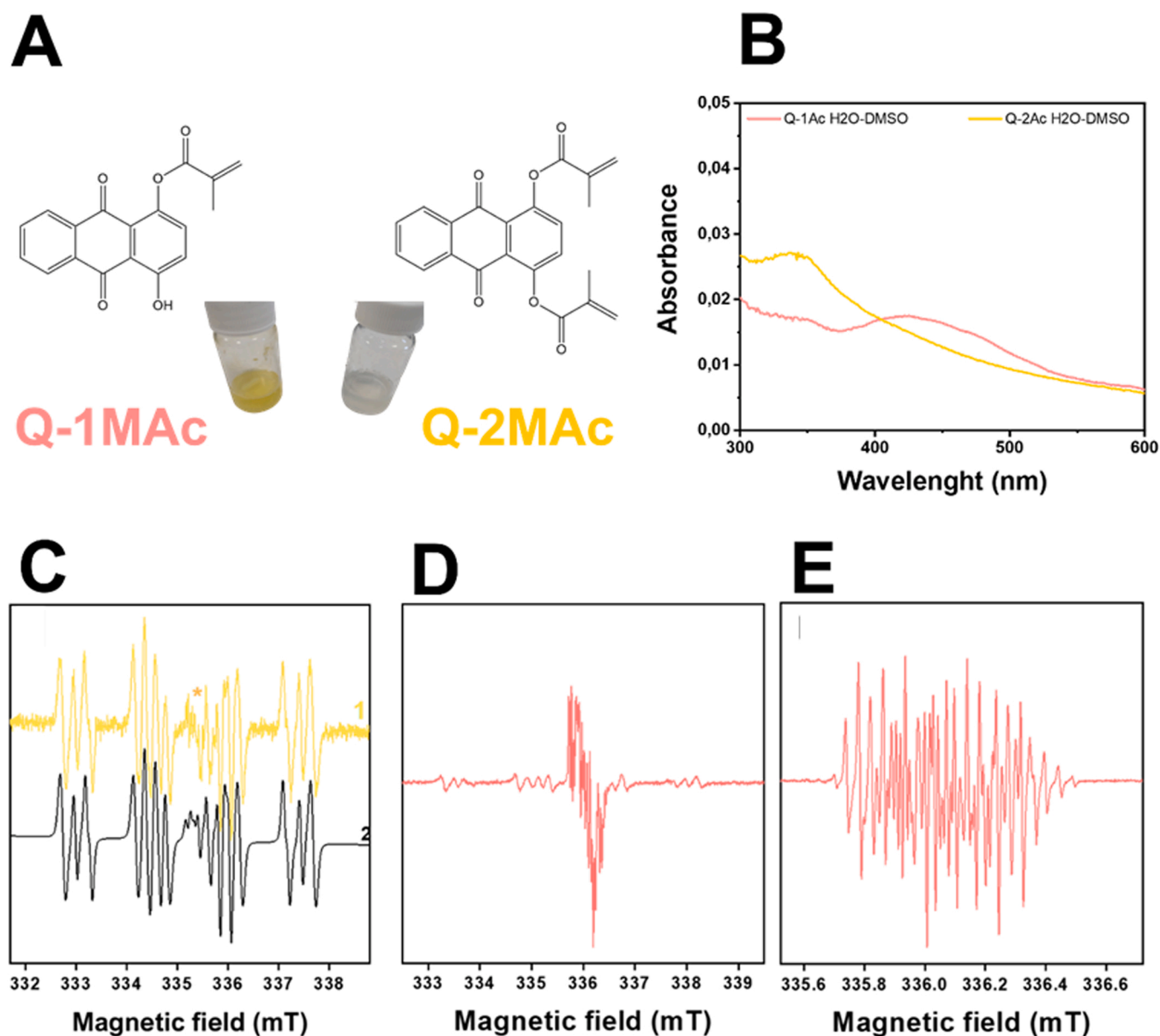
Fig. 1. Structure of the methacrylated quinizarin dyes Q-1MAc (left) and Q-2Mac (Right) and the appearance of their solution in DMSO-Water (A). UV.Vis spectra of mono-methacrylated quinizarin (Q-1MAc, pink), di-methacrylated quinizarin (Q-2MAc, yellow) (B). The normalized experimental (yellow,1) and simulated (black, 2) EPR spectra obtained during 450^{-s} in situ LED@365 nm exposure of Q-2MAc/DMSO with DMPO spin trap under argon. EPR spectrometer settings: microwave frequency, $\sim$ 9.44 GHz; microwave power, 10.01 mW; center field, $\sim$335.0 mT; sweep width, 7 mT; gain, 2.00×10^5; modulation amplitude, 0.05 mT or 0.025 mT; sweep time, 45 s; time constant, 10.24 ms; number of scans, 10. * represents the Q-2MAc-derived radical species (C). The normalized experimental EPR spectra measured during in situ LED@ 400 nm irradiation of Q-1MAc/DMSO with DMPO spin trap under argon. Exposure: (D) 225 s; (E) 450 s. EPR spectrometer settings: microwave frequency, $\sim$ 9.43 GHz; microwave power, 1.048 mW; center field, $\sim$336.1 mT; sweep width, 7 mT or 1.2 mT; gain, 1.59×10^5 or 1.00×10^4; modulation amplitude, 0.05 mT or 0.01 mT; sweep time, 45 or 90 s; time constant, 10.24 ms; number of scans, 5.

Bruker)) or with EMX*plus* spectrometer (Bruker) equipped with the High Sensitivity Probe-head (Bruker) in the small quartz flat cell (Wilmad-LabGlass, WG 808-Q). Experiments have been done in dimethylsulfoxide (DMSO, anhydrous, Sigma-Aldrich) under argon at 295 K by direct irradiation of EPR resonator using LEDs@ 365 nm or LED@ 400 nm ($\lambda_{max} = 385$ nm or 400 nm; Bluepoint LED, Hönle UV Technology). The EPR spectra were recorded in situ during/after a defined exposure time as described previously [37]. The experimental EPR spectra were analyzed by the WinEPR software (Bruker) and the calculations of spin-Hamiltonian parameters and relative concentrations of individual DMPO-adducts were performed with the EasySpin toolbox[40].

Rheological characterization. The viscosity of the formulations was evaluated with continuous flow measurements performed in

triplicate with a range of shear rate from 0,01–1000 s^{-1}, setting a gap between the two plates of 0.5 mm.

Real-time photorheological measurements were performed using an Anton PAAR Modular Compact Rheometer (Physica MCR 302, Graz, Austria) in parallel-plate mode (25 mm diameter) and the visible-light source was provided by positioning the light guide of the visible Hamamatsu LC8 lamp under the bottom plate. During the measurements, the gap between the two glass plates was set to 0.2 mm, and the sample was kept under a constant shear frequency of 1 Hz. The irradiating light was switched on after 60 s to allow the system to stabilize before the onset of polymerization. According to preliminary amplitude sweep measurements, all the tests were carried out in the linear visco-elastic region at a strain amplitude of 1 %. The photo-rheology was

Table 1

mono-methacrylated quinizarin (Q-1MAc) and di-methacrylated quinizarin (Q-2MAc) formulations prepared in water-DMSO solution 3:1. The photo-initiator concentration was chosen based on previous work [32,43]. The first column reports the abbreviated names used in the following discussion.

Sample Name	CHI-MA (wt. %)	PEGDA (wt. %)	LAP (mol/L)	Dye (mol/L)
CHI	2	–	$3 * 10^{-4}$	–
CHI-PEG	2	2	$3 * 10^{-4}$	–
CHI-PEG Q-1Mac no LAP	2	2	–	$3 * 10^{-4}$
CHI-PEG Q-2MAc no LAP	2	2	–	$3 * 10^{-4}$
CHI Q-1MAc	2	–	$3 * 10^{-4}$	$3 * 10^{-4}$
CHI-PEG Q-1MAc	2	2	$3 * 10^{-4}$	$3 * 10^{-4}$
CHI Q-2MAc	2	–	$3 * 10^{-4}$	$3 * 10^{-4}$
CHI-PEG Q-2MAc	2	2	$3 * 10^{-4}$	$3 * 10^{-4}$

studied as a function of the changes in the shear modulus (G') and in the loss modulus (G'') of the sample versus the exposure time.

Amplitude sweep tests were then performed on the cured hydrogels, the tests were carried out between 0,1 % and 1000 % of strain, frequency of 1 Hz.

Swelling properties. The different photocured samples ($\approx$ h = 3 mm, d = 5 mm) were washed and let dry overnight. Once dry, the samples were weighted and soaked in DI water to evaluate the swelling capability and kinetics. The samples were taken out at different time intervals and weighted once the surface droplets were wiped off with wet paper until constant weight. The swelling ratio (Sw %) was calculated as:

$$Sw(\%) = \frac{W_t - W_0}{W_0} * 100 \tag{1}$$

W_t is the weight of the hydrogel sample at a specific time, and W_0 is the weight of the dried sample recorded as the initial weight. All tests were performed in triplicate.

Compression test

Mechanical properties were measured by a dynamic compression test. Measurements were performed on swelled 3D printed cylindrical scaffolds ($\approx$ h = 5 mm, d = 7 mm) at 25 °C and using a universal test system, MTS QTest1/L Elite, a uniaxial testing machine equipped with a 100 N load cell in compression mode. Samples were placed between compression platens. Each sample was subsequently deformed at 1 mm/min. All measurements were performed by triplicate.

3D-printing

The 3D printing tests were performed with an Asiga PICO 2 DLP-3D printer (Asiga, Australia) equipped with a LED light source emitting at 405 nm (nominal XY pixel resolution is 39 μm, achievable Z-axis control is 1 μm). After printing, the 3D structures were soaked in distilled water for 1 min and submitted to the post-curing process performed with a mercury lamp provided by Robotfactory (10 min, light intensity 10 mW/ cm^2).

Cell viability, proliferation, and migration

Before the cell viability and proliferation assays, all the hydrogels were sterilized in a 48-well plate (Corning) as follows: three initial 10 min washes with 70 % ethanol were performed. Then, the samples were rinsed in PBS (phosphate buffer solution, Thermo Fisher) and sterilized with ultraviolet germicidal irradiation (UVGI) for 40 min. After a final rinse with PBS, the hydrogels were cover with DMEM 1X (Gibco) supplemented with 10 % FBS (fetal bovine serum, Thermo Scientific) plus antibiotics 100 U mL^{-1} penicillin and 100 μg mL^{-1} streptomycin sulphate (Sigma-Aldrich). Before the cell seeding,

hydrogels were stored immersed in the culture medium at 37ºC for 24 h. The pristine formulation of methacrylated chitosan was used as control, having already confirmed its biocompatibility in previous studies [32]. Cell assays were performed using C166-GFP mouse endothelial cell line (ATCC CRL-2583™, USA). C166-GFP were seeded over the different hydrogels with a cell concentration of 10.000cells/hydrogel, covered with 500 μL of complete culture medium and placed in an incubator at 37ºC/5 % CO$_2$. Inverted fluorescence microscopy (Olympus IX51, FITC filter λex/λem = 490/525 nm) was used daily to evaluate the culture attachment and proliferation over the surface of the hydrogels. After 72 h, metabolic activity of the cells was measured using Alamar Blue assay, following the instructions of the manufacturer (Biosource). This method is non-toxic and uses the natural reducing power of living cells, generating a quantitative measure of cell viability and cytotoxicity. Briefly, Alamar Blue dye (10 % of the culture volume) was added to each well, containing living cells seeded over hydrogels, and incubated for 90 min. Then, the fluorescence of each well was measured using a Synergy HT plate reader (BioTek) at 535/590 nm.

Finally, DNA quantitation of cells was determined by FluoReporter® Blue Fluorometric dsDNA Quantitation Kit fluorescent staining. This method is based on the ability of the bisbenzimidazole derivative Hoechst 33258 to bind to A-T-rich regions of double-stranded DNA. After binding to DNA, Hoechst 33258 exhibits an increase in fluorescence, which is measured at 360 nm excitation wavelength and 460 nm emission using a microplate reader (BioTek, Synergy HT). A t-student analysis (GraphPad Prism4) was performed to check if any statistically significant differences could be found between the different hydrogels when compared to the methacrylated chitosan control.

3. Results

3.1. Quinizarin-based dyes preliminary investigation

The structures of the two quinizarin- based molecules investigated in this study are reported in Fig. 1, A. Aiming to preliminary evaluate their properties, UV–vis absorption spectra were collected (Fig. 1, B): Q-1MAc presents a maximum absorption into the blue region (420 nm), thanks to the electron donor effect of the hydroxyl group. Contrary to Q-1Mac, the addition of a second methacrylic group on Q-2MAc moves the absorption peak to the UV region (335 nm) but maintains a moderate absorption up to 500 nm [37].

The capability of the two molecules to generate carbon-centered radicals under excitation at their maximum absorption wavelength was then studied by EPR measurements. Indeed, upon the LED@ 365 nm irradiation of Q-2MAc/DMSO solution under argon in the presence of DMPO as a spin trap, the generation of Q-2MAc-derived radical is evidenced (Fig. 1,C), along with additional EPR signals demonstrating the generation of three spin-adducts: *i)* DMPO-adduct of carbon-centered radical ($a_N = 1.450$ mT, $a_H^\beta = 2.072$ mT; $g = 2.0058$), *ii)* DMPO-adduct of acyl radical ($a_N = 1.422$ mT, $a_H^\beta = 1.637$ mT; $g = 2.0058$), and *iii)* DMPO-adduct of oxygen-centered radical ($a_N = 1.382$ mT, $a_H^\beta = 1.164$ mT, $a_H^\gamma = 0.075$ mT; $g = 2.0059$) as shown in Fig. 1,C. The LED@ 400 nm irradiation of Q-1MAc in oxygen-free DMSO solution with DMPO results in the formation of analogous three DMPO-adducts as found under analogous experimental conditions for derivative Q-2MAc (Fig. 1, C), along with the complex EPR signal of Q-1MAc-derived paramagnetic species representing superposition of Q-1MAc$^{\bullet-}$ with other Q-1MAc-derived paramagnetic species (Fig. 1, D, E).

Furthermore, envisaging the possible influence of the photoactive dyes on chitosan-based formulations, it is also important to consider that quinizarin derivatives could be implied in an electron transfer process followed by a H-abstraction reaction when combined with tertiary amine leading to the formation of aminoalkyl radical species [37]. Depending on the degree of methacrylation, CHI-MA always keeps some unreacted primary amines and, even though those amines possess lower electron donor properties, they can likely participate to the reaction as
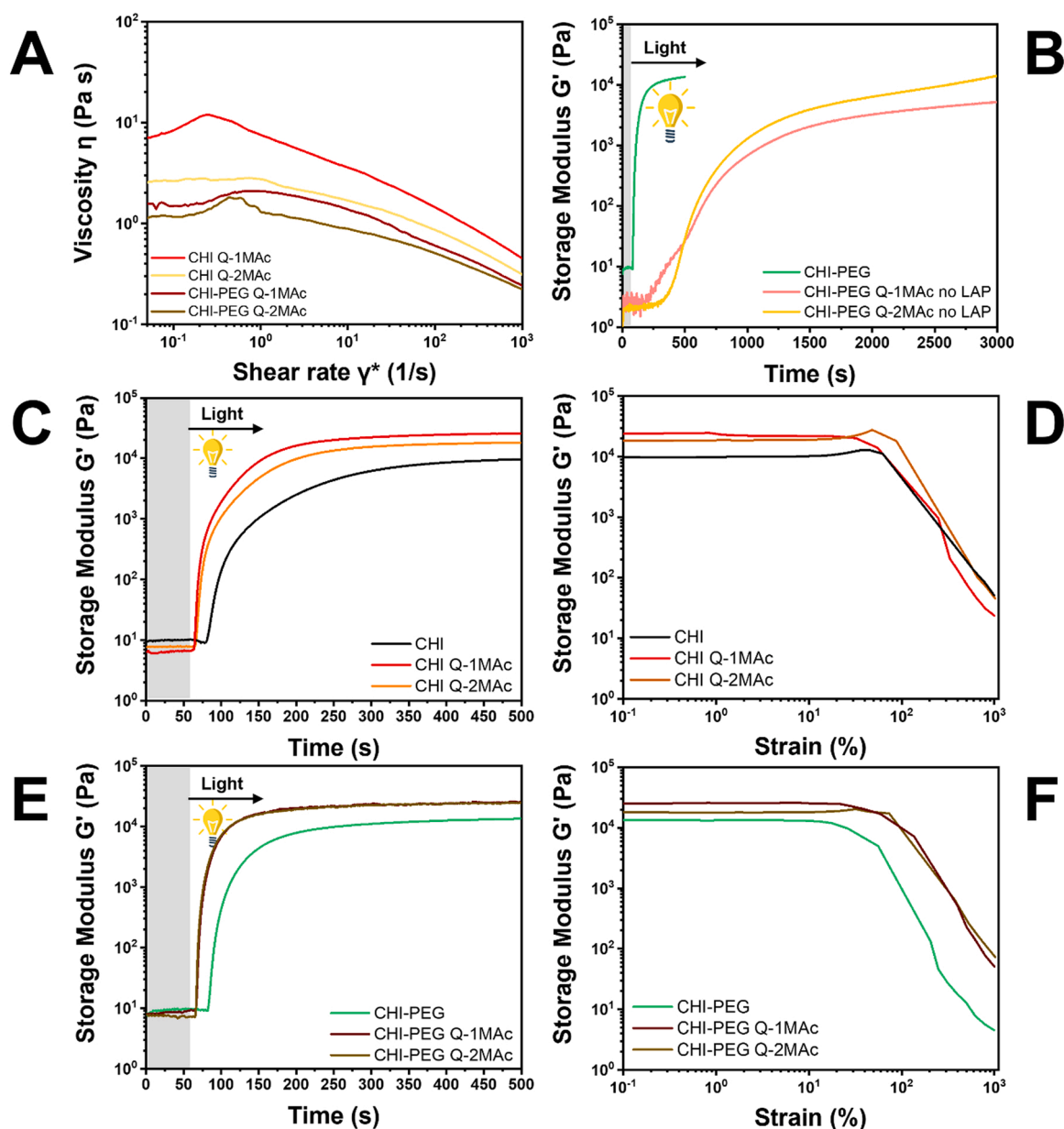
Fig. 2. Viscosity of CHI Q-1MAc, CHI Q-2MAc, CHI-PEG Q-1MAc and CHI-PEG Q-2Mac, the formulations without LAP presented the same viscosity (A), photo-rheology of compared CHI-PEG with CHI-PEG Q-1MAc no LAP and CHI-PEG Q-2MAc no LAP, the grey region indicates the part of the test performed with no light for the stabilization of the measurement (B), photo-rheology of compared CHI with CHI Q-1MAc and CHI Q-2MAc (C), amplitude sweep of compared CHI with CHI Q-1MAc and CHI Q-2MAc (D), photo-rheology of compared CHI-PEG with CHI-PEG Q-1MAc and CHI-PEG Q-2MAc (E) and amplitude sweep of compared CHI-PEG with CHI-PEG Q-1MAc and CHI-PEG Q-2MAc (F).

Table 2

Photo-rheology induction time and time-to-plateau, shear storage modulus G′, yield point, storage modulus at compression E′ and swelling percentage at the equilibrium of the reference and quinizarin-derived dyes loaded hydrogels (all the formulations contain LAP as photoinitiator).

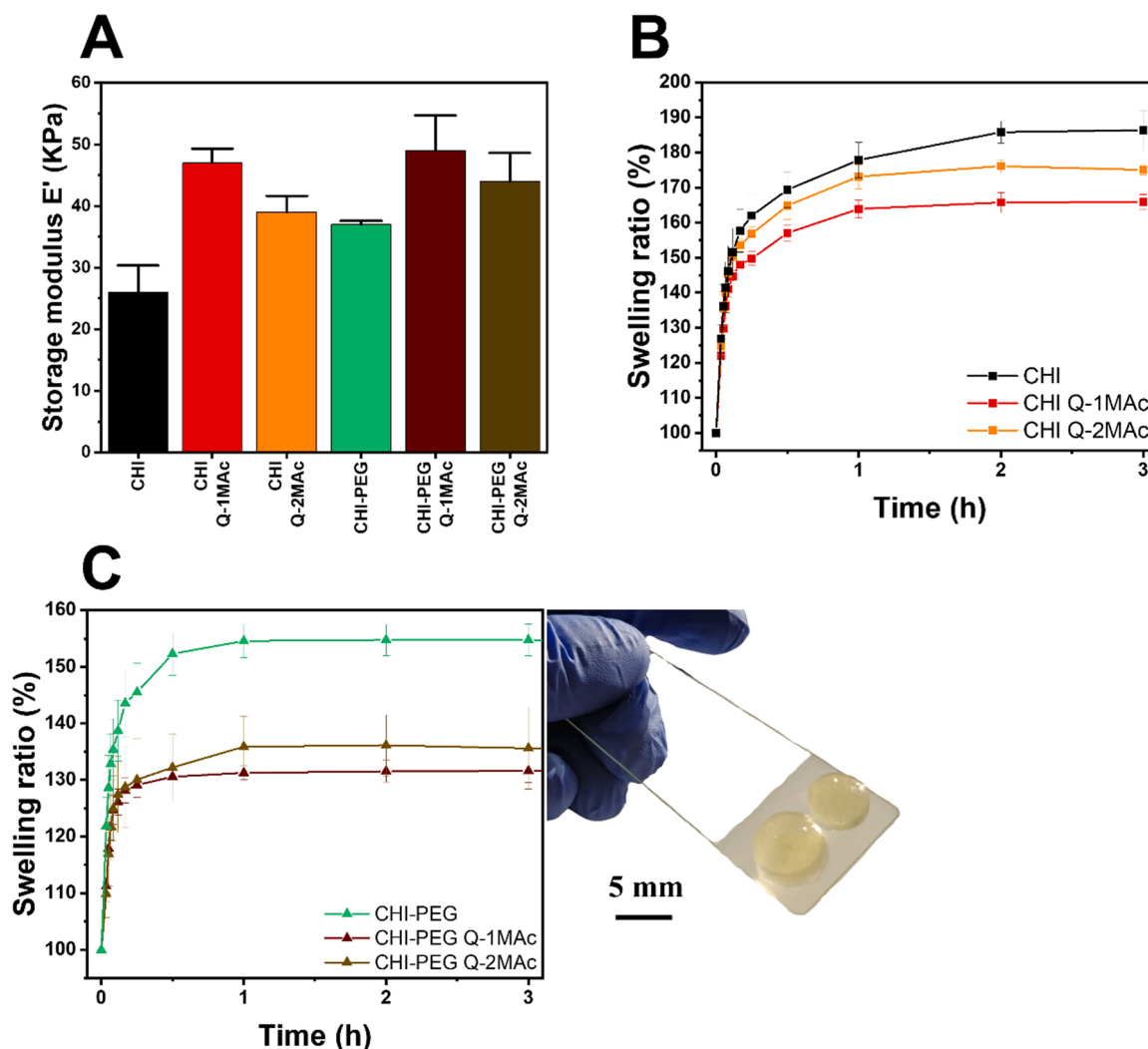| SAMPLE	Photo-rheology induction time (s)	Photo-rheology time-to-plateau (s)	Storage modulus G′ (KPa)	Yield point (%)	Elastic modulus E′ (KPa)	Swelling (%)
CHI	+20 s	none	9,9	62,5	26 ± 4	186 ± 5
CHI Q-1MAc	< 1s	185	24,1	32,1	47 ± 2	165 ± 2
CHI Q-2MAc	< 1s	193	17,8	48,2	39 ± 2	175 ± 1
CHI-PEG	+20 s	170	13,4	17,5	37 ± 1	154 ± 3
CHI-PEG Q-1MAc	< 1s	94	25,2	59,4	49 ± 5	131 ± 2
CHI-PEG Q-2MAc	< 1s	108	17,9	73,5	44 ± 4	135 ± 7

Fig. 3. Storage modulus E′ at compression (A), swelling kinetics of the CHI and CHI Quinizarin loaded formulations, (B) and swelling kinetics of the CHI-PEG and CHI-PEG Quinizarin loaded formulations with a sample before and after swelling (CHI-PEG Q-2MAc) (C).

Table 3
Optimized printing parameters of all formulation tested (all formulations contain LAP photoinitiator).

	Light intensity (mW/cm^2)	Layer thickness (μm)	Burn-in exposure time (s)	Layer exposure time (s)
CHI-PEG	25	50	10	8
CHI Q-1MAc	25	50	6	2
CHI-PEG Q-1MAc	25	50	5	1.5
CHI Q-2MAc	25	50	6	2
CHI-PEG Q-2MAc	25	50	6	1.8

co-initiators in Norrish II reactions [41–43].

3.2. Formulations development and hydrogels characterization

Two batches of formulations based on pure CHI-MA and on CHI-MA/PEGDA blends were used as reference materials for the present study. Specifically, in the case of the hybrid material, the well-known biocompatible PEGDA Mw 700 was employed as crosslinker [44,45]; the composition of the hybrid batch was empirically chosen according to preliminary tests (see SI and Table 1). LAP photo-initiator was selected as the less toxic radical photoinitiator [46] and its amount was chosen according to previous works [32,47]. Once the formulations were defined, aiming to achieve their printability, the possibility to enhance their reactivity by the addition of photo-active quinizarin-derived dyes was investigated. As demonstrated by the UV-Vis spectra, both molecules can absorb at 405 nm resulting suitable for the visible light printer in use; Q-1MAc and Q-2Mac were added in the same concentration of LAP.

For each formulation, photo-rheology, viscosity and amplitude sweep measurements were performed. These measurements offer important information for further DLP 3D experiments, Indeed, the final geometry is created upside-down in a custom fashioned layer-by-layer manner, and for this reason, the first layers need to have good reactivity in order to rapidly form a crosslinked network able to support the entire structure, while a low shear-thinning viscosity is always necessary to permit the flow of the formulation under the moving platform. At the same way, once a consistent part of the structure is formed, good mechanical properties and the ability to withstand at low solicitations or strains are required to avoid the object detaching from the platform.

Firstly, all the photosensitive formulations get viscosity values that can be considered suitable for 3D-printing [48,49] with a clear shear thinning behaviour (Fig. 2A).

Considering the photorheology tests, three main information can be extrapolated, namely: a) the induction time of the reaction (the time
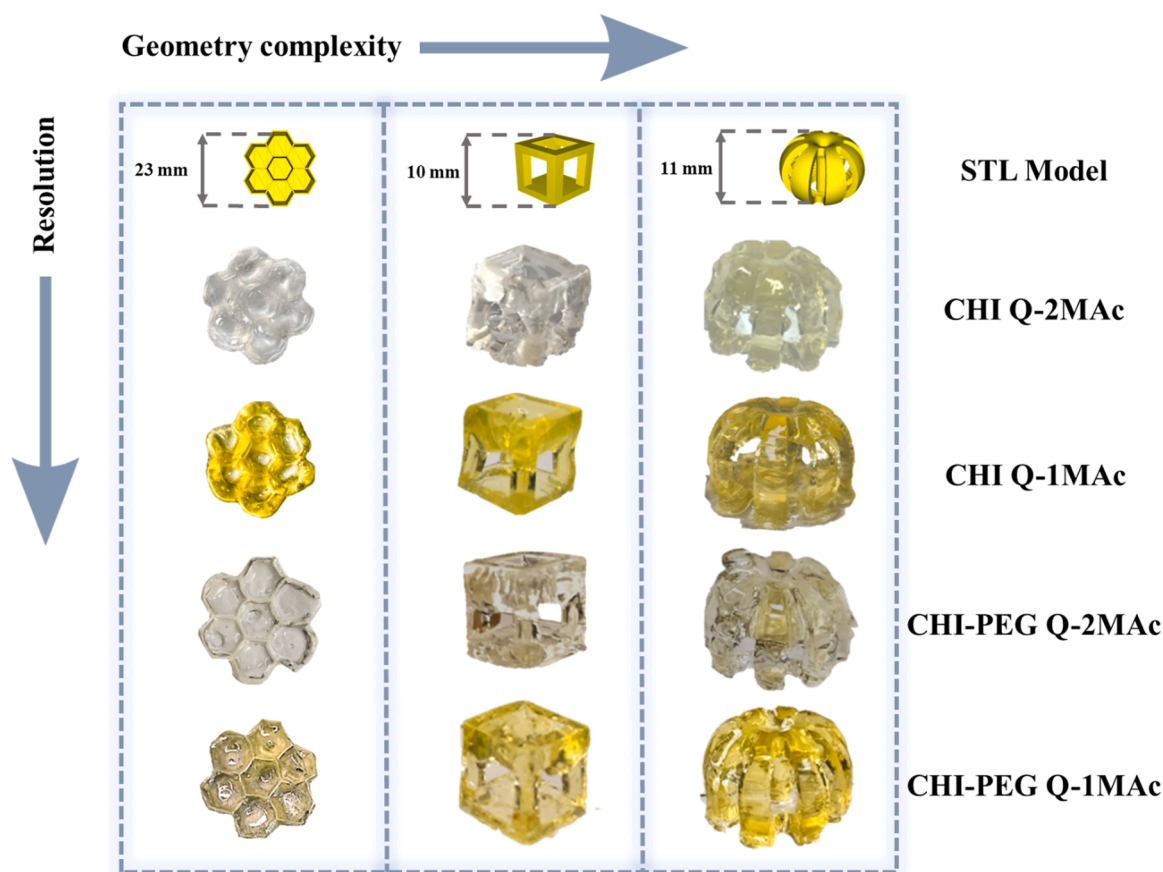
Fig. 4. Quinizarin loaded formulation 3D-printed geometries. The printed objects are reported in order of resolution (top to bottom) and geometry complexity (left to right).

where the storage modulus starts to increase) b) the rate of polymerization (suggested by the slope of the increasing curve and the time needed to reach a clear plateau) and c) the mechanical stability of the final cross-linked product (by the upper plateau value).

Two formulations based on the CHI-MA/PEGDA mixture in the presence of the two quinizarin derivatives and without the addition of any other photo-initiators (samples named CHI-PEG Q-1MAc no LAP. and CHI-PEG Q-2MAc no LAP) were firstly tested. As observed in Fig. 2B, Q-1MAc and Q-2MAc can induce the crosslinking of the hydrogels, even though demonstrating low reactivities not suitable for 3D-printing (especially because of the high crosslinking times, $\approx$ 1 h of irradiation). In particular, Q-1MAc showed an induction time of 207 s while Q-2MAc reported 312 s for the same property. However, after 500 s of irradiation, the mechanical properties of the Q-2MAc hydrogel overcome the Q-1MAc, maintaining the same trend until the end of the test. This behavior is not surprising because Q-2MAc, being dimethacrylated, can act as a crosslinker itself. At the same time, its slightly lower light absorption in the irradiation region (i.e. its lower rate of initiation) explains the increased induction time compared to Q-1MAc. Hence, the quinizarin molecules show a photoinitiating activity nevertheless the long irradiation times needed for the curing do not allow their use as single photoinitiator. Despite this, they can be used as photoactive dyes able to increase the reactiveness of the formulations when combined with common 3D photoinitiators i.e. LAP [50] making possible the DLP 3D printing of methacrylated chitosan, not achievable before. Following this path, both the quinizarin-based molecules and the LAP photo-initiator were used in the CHI-MA and CHI-MA/PEGDA based formulations to obtain the best photoreactivity. Fig. 2C and E report the photo-rheology plots of Q-1MAc and Q-2MAc solutions, respectively (compared with the previous CHI and CHI-PEG samples). As

clearly visible, the initiation of the quinizarin loaded formulations is almost instantaneous, suggesting a concomitant action of LAP and the quinizarin derivatives. A higher slope of the curves in the presence of the quinizarine-based dyes also is observed, demonstrating thus the speed up of the whole reaction. Moreover, the time-to-plateau of the different hydrogels (time needed to reach a constant plateau after the starting of the light irradiation at 60 s, see Fig. 2) is 185 s and 193 s for CHI Q-1MAc and CHI Q-2MAc samples while 94 s and 108 s are reported for samples CHI-PEG Q-1MAc and CHI-PEG Q-2MAc, both confirming an increased reactiveness. PEGDA or CHI-MA chains can likely act as H-donor molecule, as previously demonstrated with Eosin-PEG formulations [51]. In the same way, quinizarin derivatives can also act as type II photo-initiators and abstract proton from PEGDA or CHI-MA backbone, leading to the formation of initiating carbon-centered radicals.

The mechanical properties, the stability of the hydrogels, and their possibility to withstand over low solicitations or strains are tested by amplitude sweep and compression tests. The amplitude sweep storage modulus and yield points (Fig. 2D and F, reported on Table 2) demonstrate the mechanical stability of these materials at relatively high % strain compared to the corresponding CHI and CHI-PEG samples, while maintaining an higher G′ modulus. At the same way, the E′ compressive storage modulus calculated in the first 10 % of deformation in the stress-strain curve (Fig. 3A, reported on Table 2) indicates increased mechanical properties, in line with previously reported chitosan-based hydrogels [32] and with values comparable to soft tissues [52,53].

For the swelling test, the different formulations were casted into PDMS moulds and irradiated to create cylindrical hydrogels that were left dry overnight. Once dried the samples were weighted and soaked in DI water to evaluate the swelling capability and swelling kinetics. Fig. 3 B and C report the swelling kinetics of the quinizarin loaded hydrogel
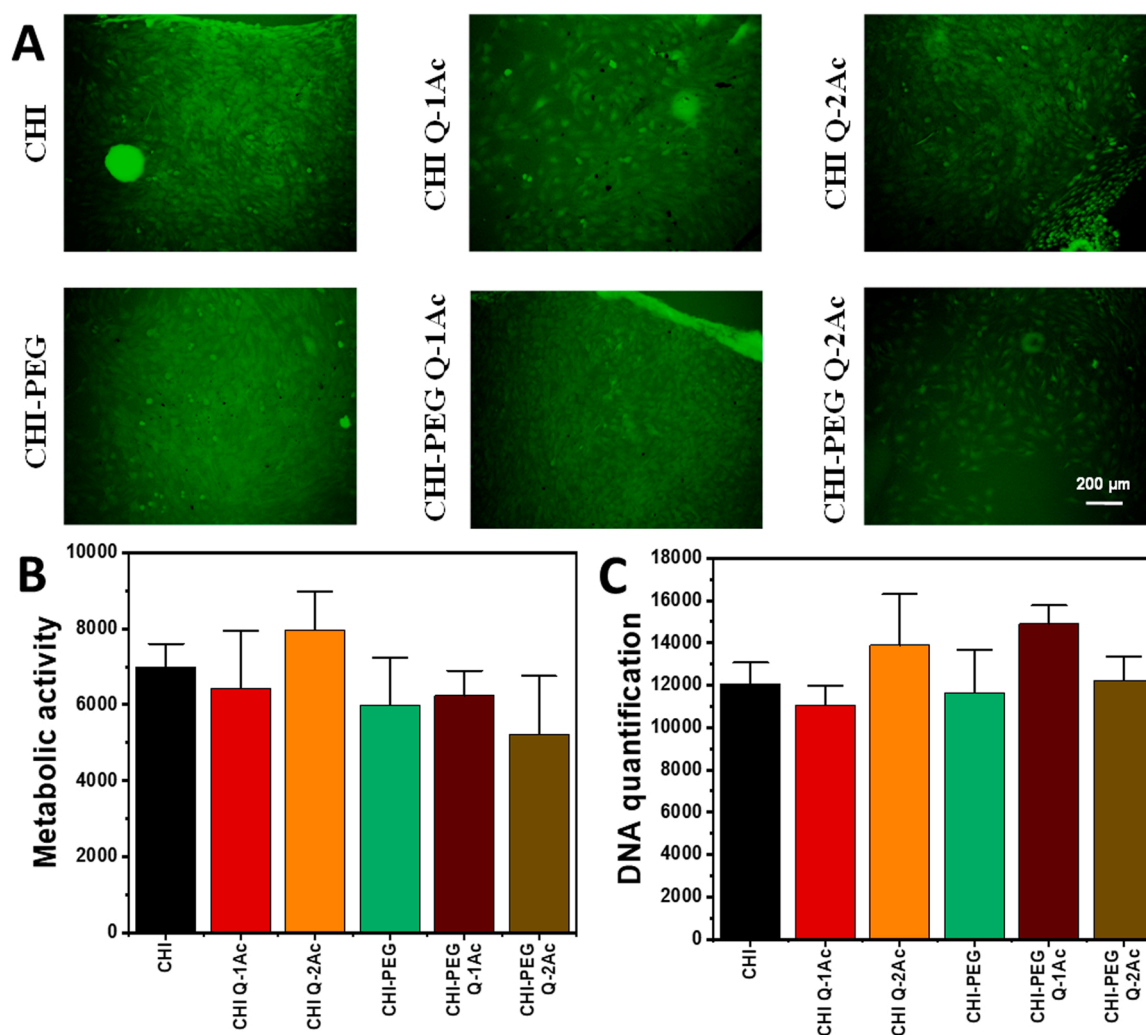
Fig. 5. (A) Micrographs of C166-GFP murine endothelial cells on the surface of the different hydrogels after 72 h of incubation, (B) Metabolic activity values of the C166 cell cultures for the different hydrogels after 72 h of incubation, (C) DNA quantitation values of C166 cell cultures for the different hydrogels after 72 h of incubation.

(compared with the CHI and CHI-PEG samples swelling kinetics) while in Table 2 are expressed their swelling equilibrium. No differences in the time needed to complete swelling was evidenced (≈ 2 h for the CHI-MA based hydrogels and 1 h for the CHI-MA/PEGDA based ones), while a decrease in the swelling equilibrium resulted when the two methacrylated molecules were added. This behaviour can be justified both with an increased crosslinking density (as demonstrated by the higher G′ modulus) and the quinizarin low affinity with water.

3.3. 3D printing of the quinizarin-derived formulations

All the formulations reported in Table 1 containing LAP were tested for DLP printing; three different geometries with increasing complexity were selected (i.e., honeycomb, hollow cube and light fountain). In particular, the 2.5 D honeycomb structure, with no suspended structures, was selected as the minimum criteria to define a formulation DLP printable, the hollow cube to evaluate the structure stability and the angles shape fidelity while the rounded 3D cad is experimented to test the ink's complex and interconnected internal hollow geometries creation. The printability of the reference formulations without the quinizarin dyes was firstly evaluated: neat methacrylated chitosan presented a too low reactivity and poor mechanical properties to be printed, while the CHI-MA/PEGDA based formulation gave materials with slightly better properties. Nevertheless, the first printing attempts without using

any dye leaded to overcured structures so, aiming to assure a reasonable resolution [36], a common water-soluble and visible light absorber dye (brilliant green) was added to the CHI-MA/PEGDA formulation (see SI). This last formulation allowed the printing of the honeycomb structure with limited resolution (see SI) while more complicated architectures, such as hollow cubes, were impossible to print cause of a collapse and a detach of the structure from the building platform.

On the contrary, the use of the quinizarin-derived molecules enabled the DLP printing of more complex structures.

Table 3 reports the optimized printing parameters: since each formulation possess different reactivity (Fig. 2C and E) these parameters are the minimum printing times able to create a self-standing geometry. As demonstrated in Fig. 4, all the printing attempts lead to defined and recognizable structures and, depending on the formulation, increasing levels of resolution. Moreover, reduced printing times compared with the CHI-PEG samples were evidenced, certifying what already observed during photo-rheology. As expected, the PEGDA charged solutions (96 wt. % of water) lead to more detailed geometries with well-shaped angles and dimensions. As expected, also the CHI-MA formulations (CHI Q-1MAc or CHI Q-2MAc, 98 wt. % of water) result in well-shaped and self-standing architectures with defined angles for the CHI Q-1MAc hydrogel. The visible light-centred absorption of Q-1MAc and its influence on the crosslinking kinetics (Fig. 2C) explain the higher resolution of the corresponding 3D-printed hydrogels compared to Q-2MAc ones.

This behaviour is also responsible for the increased mechanical properties of the mono-methacrylated biomolecules suggesting Q-1MAc as the best candidate for visible-light 3D printing.

3.4. Cell proliferation over 3D-printed hydrogels

Autofluorescent C166-GFP endothelial cells were seeded over the different hydrogels to assess their cytocompatibility. The cytocompatibility of light-cured CHI-MA based hydrogels was previously demonstrated [32] thus, the main objective of the tests was investigating the influence of the quinizarin based dyes on this behaviour. Fig. 5A shows the fluorescence micrographs after 72 h of contact for the studied samples. The cells appear adhered, forming a monolayer and no evidence of cell death was observed. All the hydrogels showed normal parameters of adhesion, size and morphology expected for endothelial cells, from 24 h to 72 h of growth (Fig. S6), reaching confluency in all samples after three days of growth. To quantify this excellent behaviour, metabolic activity (Alamar Blue) and DNA contempt (Fluoreporter) assays were performed (Fig. 5B and C, respectively). The higher values in terms of viability and growth were achieved with the CHI Q-2MAc hydrogel, probably cause a better incorporation inside of the chitosan network due to both its methacrylated extremities [54]. However, the trend extracted from the data was very similar for all the samples in both tests, with no statistically significant differences among the different hydrogels. In conclusion, the use of quinizarin based dyes improves the printability of methacrylated chitosan and does not limit the cytocompatibility of the original material.

4. Conclusions

The 3D-printing of methacrylated chitosan complex geometries was successfully performed loading the initial formulations with mono- and di-methacrylated quinizarin-derivatives, granting the detailed printability of solo-methacrylated chitosan geometries (98 wt. % of water, not possible in absence of the quinizarin molecules) and the defined printability of the poly(ethylene glycol) charged methacrylated chitosan formulations. Moreover, the functionalities of the bio-derived quinizarin-derivative as photo active molecules and dye were demonstrated. The resulted structures possess suitable mechanical properties, mechanical stability and swelling capability/kinetics to be employed as soft scaffold for tissue engineering. The exhibited reactivity under visible light and the null cytotoxicity allows cell proliferation, as distinguishable by the metabolic activity and DNA quantification of the cells seeded hydrogels. In conclusion, the smart employment of photo-active dyes, not only as light-scattering preventers, but also as useful and participating agents in the 3D-printing could increase the possibility to create engineered tissues perfectly designed and tailored on the patient's requirements.

CRediT authorship contribution statement

Michael Zanon Investigation, Formal analysis, Writing – Original Draft, Visualization. **Raquel Cue-López** Investigation, Formal anlysis. **Enrique Martínez-Campos** Validation, Writing – Review & Editing. **Paula Bosch**, Validation, Resources, Writing – Review & Editing. **Davy-Louis Versace** Validation, Writing – Review & Editing. **Hassan Hayek**, Investigation, Formal analysis. **Nadia Garino**, Validation, Writing – Review & Editing. **Candido Fabrizio Pirri** Resources, Supervision. **Marco Sangermano**, Supervision. **Annalisa Chiappone*** Conceptualization, Validation, Visualization, Writing – Review & Editing.

Declaration of Competing Interest

The authors declare that they have no known competing financial interests or personal relationships that could have appeared to influence the work reported in this paper.

Data Availability

Data will be made available on request.

Acknowledgments

Appendix A. Supporting information

Supplementary data associated with this article can be found in the online version at doi:10.1016/j.addma.2023.103553.

References

[1] E.M. Maines, M.K. Porwal, C.J. Ellison, T.M. Reineke, Sustainable advances in SLA/DLP 3D printing materials and processes, Green. Chem. 23 (18) (2021) 6863–6897.

[2] M. Shahbazi, H. Jäger, Current status in the utilization of biobased polymers for 3D printing process: a systematic review of the materials, processes, and challenges, ACS Appl. Bio Mater. 4 (1) (2021) 325–369.

[3] V.S.D. Voet, J. Guit, K. Loos, Sustainable photopolymers in 3d printing: a review on biobased, biodegradable, and recyclable alternatives, Macromol. Rapid Commun. 42 (3) (2021) 2000475.

[4] C.W. Hull, S.T. Spence, D.J. Albert, D.R. Smalley, R.A. Harlow, P. Steinbaugh, H.L. Tarnoff, H.D. Nguyen, C.W. Lewis, T.J. Vorgitch, Methods and apparatus for production of three-dimensional objects by stereolithography, Google Pat. (1991).

[5] M. Pagac, J. Hajnys, Q.-P. Ma, L. Jancar, J. Jansa, P. Stefek, J. Mesicek, A review of vat photopolymerization technology: materials, applications, challenges, and future trends of 3D printing, Polymers 13 (4) (2021) 598.

[6] A. Cortés, A. Cosola, M. Sangermano, M. Campo, S. González Prolongo, C.F. Pirri, A. Jiménez-Suárez, A. Chiappone, D.L.P. 4D-Printing, 4D-Printing of remotely, modularly, and selectively controllable shape memory polymer nanocomposites embedding carbon nanotubes, Adv. Funct. Mater. 31 (50) (2021) 2106774.

[7] M. Mukhtarkhanov, A. Perveen, D. Talamona, Application of stereolithography based 3D printing technology in investment casting, Micro (Basel) 11 (10) (2020).

[8] S.C. Joshi, A.A. Sheikh, 3D printing in aerospace and its long-term sustainability, Virtual Phys. Prototyp. 10 (4) (2015) 175–185.

[9] N. Bhattacharjee, A. Urrios, S. Kang, A. Folch, The upcoming 3D-printing revolution in microfluidics, Lab a Chip 16 (10) (2016) 1720–1742.

[10] C. Noè, C. Tonda-Turo, A. Chiappone, M. Sangermano, M. Hakkarainen, Light processable starch hydrogels, Polymers 12 (6) (2020) 1359.

[11] R. Laurano, C. Cassino, G. Ciardelli, V. Chiono, M. Boffito, Polyurethane-based thiomers: a new multifunctional copolymer platform for biomedical applications, React. Funct. Polym. 146 (2020), 104413.

[12] D. Lei, Y. Yang, Z. Liu, B. Yang, W. Gong, S. Chen, S. Wang, L. Sun, B. Song, H. Xuan, X. Mo, B. Sun, S. Li, Q. Yang, S. Huang, S. Chen, Y. Ma, W. Liu, C. He, B. Zhu, E.M. Jeffries, F.-L. Qing, X. Ye, Q. Zhao, Z. You, 3D printing of biomimetic vasculature for tissue regeneration, Mater. Horiz. 6 (6) (2019) 1197–1206.

[13] B. Grigoryan, S.J. Paulsen, D.C. Corbett, D.W. Sazer, C.L. Fortin, A.J. Zaita, P.T. Greenfield, N.J. Calafat, J.P. Gounley, A.H. Ta, F. Johansson, A. Randles, J.E. Rosenkrantz, J.D. Louis-Rosenberg, P.A. Galie, K.R. Stevens, J.S. Miller, Multivascular networks and functional intravascular topologies within biocompatible hydrogels, Science 364 (6439) (2019) 458–464.

[14] R.A.A. Muzzarelli, Chitins and chitosans for the repair of wounded skin, nerve, cartilage and bone, Carbohydr. Polym. 76 (2) (2009) 167–182.

[15] Y. Yang, L. Xu, J. Wang, Q. Meng, S. Zhong, Y. Gao, X. Cui, Recent advances in polysaccharide-based self-healing hydrogels for biomedical applications, Carbohydr. Polym. 283 (2022), 119161.

[16] S.A. Sell, P.S. Wolfe, K. Garg, J.M. McCool, I.A. Rodriguez, G.L. Bowlin, Polymers (2010) 522–553.

[17] C. Shi, Y. Zhu, X. Ran, M. Wang, Y. Su, T. Cheng, Therapeutic potential of chitosan and its derivatives in regenerative medicine1 1 this work was supported by "973″ programs on severe trauma (NO. 1999054205 and NO. 2005CB522605) from the Ministry of Science and Technology of China, J. Surg. Res. 133 (2) (2006) 185–192.

[18] Z. Feng, M. Hakkarainen, H. Grützmacher, A. Chiappone, M. Sangermano, Photocrosslinked chitosan hydrogels reinforced with chitosan-derived nano-graphene oxide, Macromol. Chem. Phys. 220 (13) (2019) 1900174.

[19] Y. Liang, Z. Wu, Y. Wei, Q. Ding, M. Zilberman, K. Tao, X. Xie, J. Wu, Self-healing, self-adhesive and stable organohydrogel-based stretchable oxygen sensor with high performance at room temperature, Nano-Micro Lett. 14 (1) (2022) 52.

[20] C. Wei, X. Jin, C. Wu, W. Zhang, Injectable composite hydrogel based on carbon particles for photothermal therapy of bone tumor and bone regeneration, J. Mater. Sci. Technol. 118 (2022) 64–72.

[21] M. Rajabi, M. McConnell, J. Cabral, M.A. Ali, Chitosan hydrogels in 3D printing for biomedical applications, Carbohydr. Polym. 260 (2021) 117768.

[22] L. Zhou, H. Ramezani, M. Sun, M. Xie, J. Nie, S. Lv, J. Cai, J. Fu, Y. He, 3D printing of high-strength chitosan hydrogel scaffolds without any organic solvents, Biomater. Sci. 8 (18) (2020) 5020–5028.

[23] C. Tonda-Turo, I. Carmagnola, A. Chiappone, Z. Feng, G. Ciardelli, M. Hakkarainen, M. Sangermano, Photocurable chitosan as bioink for cellularized therapies towards personalized scaffold architecture, Bioprinting 18 (2020), e00082.

[24] H.K. Chang, D.H. Yang, M.Y. Ha, H.J. Kim, C.H. Kim, S.H. Kim, J.W. Choi, H. J. Chun, 3D printing of cell-laden visible light curable glycol chitosan bioink for bone tissue engineering, Carbohydr. Polym. 287 (2022), 119328.

[25] T.T. Demirtaş, G. Irmak, M. Gümüşderelioğlu, A bioprintable form of chitosan hydrogel for bone tissue engineering, Biofabrication 9 (3) (2017), 035003.

[26] K.D. Roehm, S.V. Madihally, Bioprinted chitosan-gelatin thermosensitive hydrogels using an inexpensive 3D printer, Biofabrication 10 (1) (2017), 015002.

[27] M. Sahranavard, A. Zamanian, F. Ghorbani, M.H. Shahrezaee, A critical review on three dimensional-printed chitosan hydrogels for development of tissue engineering, Bioprinting 17 (2020), e00063.

[28] F. Zhang, L. Zhu, Z. Li, S. Wang, J. Shi, W. Tang, N. Li, J. Yang, The recent development of vat photopolymerization: a review, Addit. Manuf. 48 (2021), 102423.

[29] C.A. Murphy, K.S. Lim, T.B.F. Woodfield, Next evolution in organ-scale biofabrication: bioresin design for rapid high-resolution vat polymerization, Adv. Mater. 34 (20) (2022) 2107759.

[30] S.H. Kim, Y.K. Yeon, J.M. Lee, J.R. Chao, Y.J. Lee, Y.B. Seo, M.T. Sultan, O.J. Lee, J. S. Lee, Precisely printable and biocompatible silk fibroin bioink for digital light processing 3D printing, Nat. Commun. 9 (1) (2018) 1620.

[31] O.M. Kolawole, W.M. Lau, V.V. Khutoryanskiy, Methacrylated chitosan as a polymer with enhanced mucoadhesive properties for transmucosal drug delivery, Int. J. Pharm. 550 (1) (2018) 123–129.

[32] M. Zanon, A. Chiappone, N. Garino, M. Canta, F. Frascella, M. Hakkarainen, C. F. Pirri, M. Sangermano, Microwave-assisted methacrylation of chitosan for 3D printable hydrogels in tissue engineering, Mater. Adv. 3 (1) (2022) 514–525.

[33] Y. Shen, H. Tang, X. Huang, R. Hang, X. Zhang, Y. Wang, X. Yao, DLP printing photocurable chitosan to build bio-constructs for tissue engineering, Carbohydr. Polym. 235 (2020), 115970.

[34] Y. He, F. Wang, X. Wang, J. Zhang, D. Wang, X. Huang, A photocurable hybrid chitosan/acrylamide bioink for DLP based 3D bioprinting, Mater. Des. 202 (2021), 109588.

[35] Y. Lu, F. Wang, Q. Shi, J. Zhang, Z. Xiang, N. Li, X. Huang, J. Song, Three-dimensional printing chitosan-based bolus used for radiotherapy, ACS Appl. Bio Mater. 4 (9) (2021) 7094–7102.

[36] M. Gastaldi, F. Cardano, M. Zanetti, G. Viscardi, C. Barolo, S. Bordiga, S. Magdassi, A. Fin, I. Roppolo, Functional dyes in polymeric 3D printing: applications and perspectives, ACS Mater. Lett. 3 (1) (2021) 1–17.

[37] L. Breloy, V. Brezová, Z. Barbieriková, Y. Ito, J. Akimoto, A. Chiappone, S. Abbad-Andaloussi, J.-P. Malval, D.-L. Versace, Methacrylated quinizarin derivatives for visible-light mediated photopolymerization: promising applications in 3D-printing biosourced materials under LED@405 nm, ACS Appl. Polym. Mater. 4 (1) (2022) 210–228.

[38] V. Ansteinsson, H.B. Kopperud, E. Morisbak, J.T. Samuelsen, Cell toxicity of methacrylate monomers-The role of glutathione adduct formation, J. Biomed. Mater. Res. - Part A 101 (2013) 3504–3510, https://doi.org/10.1002/jbm. a.34652.

[39] M. Suh, D. Proctor, G. Chappell, J. Rager, C. Thompson, S. Borghoff, L. Finch, R. Ellis-Hutchings, K. Wiench, A review of the genotoxic, mutagenic, and carcinogenic potentials of several lower acrylates, Toxicology 402–403 (2018) 50–67, https://doi.org/10.1016/j.tox.2018.04.006.

[40] S. Stoll, A. Schweiger, EasySpin, a comprehensive software package for spectral simulation and analysis in EPR, J. Magn. Reson. 178 (1) (2006) 42–55.

[41] A. Cosola, A. Chiappone, C. Martinengo, H. Grützmacher, M. Sangermano, Gelatin type A from porcine skin used as co-initiator in a radical photo-initiating system, Polymers (Basel) 11 (2019) 1–9, https://doi.org/10.3390/polym11111901.

[42] M. Zanon, D. Baruffaldi, M. Sangermano, C.F. Pirri, F. Frascella, A. Chiappone, Visible light-induced crosslinking of unmodified gelatin with PEGDA for DLP-3D printable hydrogels, Eur. Polym. J. 160 (2021), 110813.

[43] J. Wu, P.S. Grant, X. Li, A. Noble, V.K. Aggarwal, Catalyst-free deaminative functionalizations of primary amines by photoinduced single-electron transfer, Angew. Chem. Int. Ed. 58 (17) (2019) 5697–5701.

[44] C. Warr, J.C. Valdoz, B.P. Bickham, C.J. Knight, N.A. Franks, N. Chartrand, P. M. Van Ry, K.A. Christensen, G.P. Nordin, A.D. Cook, Biocompatible PEGDA resin for 3D printing, ACS Appl. Bio Mater. 3 (4) (2020) 2239–2244.

[45] B.D. Fairbanks, M.P. Schwartz, C.N. Bowman, K.S. Anseth, Photoinitiated polymerization of PEG-diacrylate with lithium phenyl-2,4,6-trimethylbenzoylphosphinate: polymerization rate and cytocompatibility, Biomaterials 30 (35) (2009) 6702–6707.

[46] T. Majima, W. Schnabel, W. Weber, Phenyl-2,4,6-trimethylbenzoylphosphinates as water-soluble photoinitiators. Generation and reactivity of O͞P(C6H5)(O−) radical anions, Die Makromol. Chem. 192 (1991) 2307–2315, http://doi.wiley. com/10.1002/macp.1991.021921010.

[47] B. Huber, K. Borchers, G.E.M. Tovar, P.J. Kluger, Methacrylated gelatin and mature adipocytes are promising components for adipose tissue engineering, J. Biomater. Appl. 30 (6) (2015) 699–710.

[48] R.-Z. Lin, Y.-C. Chen, R. Moreno-Luna, A. Khademhosseini, J.M. Melero-Martin, Transdermal regulation of vascular network bioengineering using a photopolymerizable methacrylated gelatin hydrogel, Biomaterials 34 (28) (2013) 6785–6796.

[49] D. Cafiso, A.A. Septevani, C. Noè, T. Schiller, C.F. Pirri, I. Roppolo, A. Chiappone, 3D printing of fully cellulose-based hydrogels by digital light processing, Sustain. Mater. Technol. 32 (2022), e00444.

[50] M. Maturi, C. Pulignani, E. Locatelli, V. Vetri Buratti, S. Tortorella, L. Sambri, M. Comes Franchini, Phosphorescent bio-based resin for digital light processing (DLP) 3D-printing, Green Chem. 22 (18) (2020) 6212–6224.

[51] M.C. DeRosa, R.J. Crutchley, Photosensitized singlet oxygen and its applications, Coord. Chem. Rev. 233–234 (2002) 351–371.

[52] P. Sautrot-Ba, A. Contreras, S. Abbad Andaloussi, T. Coradin, C. Hélary, N. Razza, M. Sangermano, P.E. Mazeran, J.P. Malval, D.L. Versace, Eosin-mediated synthesis of polymer coatings combining photodynamic inactivation and antimicrobial properties, J. Mater. Chem. B 5 (36) (2017) 7572–7582.

[53] V.C. Shukla, N. Higuita-Castro, P. Nana-Sinkam, S.N. Ghadiali, Substrate stiffness modulates lung cancer cell migration but not epithelial to mesenchymal transition, J. Biomed. Mater. Res. Part A 104 (5) (2016) 1182–1193.

[54] B. Bhana, R.K. Iyer, W.L. Chen, R. Zhao, K.L. Sider, M. Likhitpanichkul, C. A. Simmons, M. Radisic, Influence of substrate stiffness on the phenotype of heart cells, Biotechnol. Bioeng. 105 (6) (2010), 1148-60.